Research on Sparse Imaging Method of Electrical Impedance Tomography Based on DK-SVD

Qi Wang[1], Xin Ding[1], Ming Ma[2, *], Xiuyan Li[1], Xiaojie Duan[1], and Jianming Wang[1]

Abstract—As a noninvasive imaging technique for the interior of objects, Electrical Impedance Tomography (EIT) is widely used in many fields of biomedicine. Sparse reconstruction algorithms have made major breakthroughs in the field of image reconstruction in recent years. The K-SVD algorithm is an adaptive dictionary signal sparse representation algorithm, which could improve the reconstruction accuracy. However, the parameters in the K-SVD algorithm are fixed, which cannot match all the measurement data of EIT very well. Moreover, the K-SVD algorithm adopts a greedy algorithm in the sparse coding stage, which has high computational complexity. In this study, an electrical impedance sparse imaging method based on DK-SVD (deep k-singular value decomposition) was designed. It provides the corresponding optimal model parameters for each set of measurement data through the method of multi-layer perceptron (MLP) network training, thereby improving the imaging quality. At the same time, the iterative soft threshold algorithm (ISTA) is used in the sparse coding stage to improve the convergence speed. The reconstruction results show that compared with the KSVD algorithm and Total Variation (TV) algorithm, the reconstruction error of the DK-SVD method is smaller, and the irregular and sharp inclusions can be accurately reconstructed. Image artifacts are also greatly reduced.

1. INTRODUCTION

Electrical Impedance Tomography (EIT) is known as a noninvasive, low-cost, zero-radiation, and easy-to-operate functional imaging technique inside objects. EIT has been applied in many practical applications, e.g., detection of breast cancer, localization of epilepsy foci, chest EIT imaging, and functional lung imaging during mechanical ventilation [1–4].

The EIT imaging problem is understood as a nonlinear problem, which is underdetermined and ill-conditioned. Measurement noise can easily affect the quality of the reconstructed image. Therefore, it is of great significance to mine the effective information from the measurement data and further improve the imaging quality. In recent years, sparse reconstruction methods based on compressed sensing theory have attracted extensive attention in the field of image reconstruction [5–7]. Reconstruction of high-resolution imaging or signals from small amounts of data is allowed in this theory.

The exact determination of the sparsest representations proves to be an NP-hard problem [8]. Thus, approximate solutions are considered instead. A sparse dictionary is an overcomplete dictionary composed of standard orthonormal bases. Efficient selection of a sparse dictionary is the key to accurate EIT sparse reconstruction. A K-SVD algorithm has been proposed to make the designed dictionary fit the sparse model better [9]. The purpose of the method is to use the generalized k-means clustering to enable dictionary learning to be done so that the image reconstruction quality is improved [10, 11]. At present, the K-SVD algorithm has been used in EIT reconstruction, which can reduce reconstruction

[1] School of Electronic and Information Engineering, Tiangong University, Tianjin 300387, China. [2] School of Life Science, Tiangong University, Tianjin 300387, China.

artifacts and noise [12, 13]. However, image reconstruction using the K-SVD algorithm also creates problems: (1) The regularization parameters in the dictionary learning process need to be adjusted manually. (2) A simple tracking algorithm is used in the sparse coding stage, making the pseudo-inverse operation of the matrix very inefficient.

Inspired by the application of the deep learning method in EIT imaging [14], this paper proposes an EIT sparse reconstruction algorithm based on deep learning adaptive adjustment parameters, namely DK-SVD (deep k-singular value decomposition). Aiming at the problem that the EIT image reconstruction process is sensitive to the measurement data of different conductivity distributions, the algorithm establishes the mapping between the measurement data and the model parameters. The optimal regularization parameters are assigned to each image patch using the MLP network. The parameter mismatch problem caused by K-SVD fixed parameters is avoided. In the sparse coding stage, the ISTA algorithm based on l_1 norm is used instead of the greedy algorithm, which makes the convergence speed faster and the reconstruction speed faster. In addition, the DK-SVD algorithm inherits the advantages of the KSVD algorithm in the process of dictionary learning. That is, sparse coding based on the current dictionary and the dictionary atoms updating alternate to better fit the data. This method aims to build a bridge between the deep learning network and the traditional sparse reconstruction algorithm so that the advantages of the two kinds of algorithms can be integrated and displayed to the greatest extent.

This paper is organized as follows. In Section 2, background and related work are introduced. In Section 3, a model based on DK-SVD is constructed. In Section 4, the DK-SVD algorithm is evaluated. The results show that the new method could achieve better image quality. In Section 5, the conclusions and future research directions are presented.

2. BACKGROUND AND RELATED WORK

The EIT image reconstruction problem can also be understood as the EIT inverse problem. To solve the EIT inverse problem, common image reconstruction algorithms are generally divided into iterative algorithms and non-iterative algorithms [15–18]. As an iterative algorithm, the sparse reconstruction method has the advantage of strong edge preservation.

In recent years, sparse algorithms have been widely applied to medical and industrial fields and achieved good results [19–27]. Based on sparse decomposition and signal approximation, the theoretical framework of compressed sensing was established [28]. The advantage of this theory is that data are properly compressed while signals are acquired, thereby saving storage space. However, it is difficult to guarantee the sparsity and quality of reconstructed images by directly applying the sparsity-promoting methods based on a conventional EIT model [29]. The sparsity of EIT images in some transform domains (finite differences, wavelets, contourlets, etc.) is the key to accurate sparse reconstruction [30]. Since the l_1 regularization method tends to produce a sparse solution, it is always used for sparse reconstruction of EIT.

Adaptive dictionaries can sparsify images better since they are learnt for the particular class of images or image instance. The shift from global to patch image sparsity effectively reduces noise and artifacts in EIT without sacrificing resolution [31, 32]. K-SVD algorithm is a dictionary learning method in which the sparse dictionary is optimized during iteration. K-SVD algorithm no longer updates the entire dictionary at one time but updates the dictionary column by column. Therefore, the reconstruction accuracy is greatly improved.

We have used K-SVD algorithm for dictionary learning in EIT reconstruction [33]. However, the EIT image reconstruction process is sensitive to the measurement data of different conductivity distributions, and the fixed regularization parameter in the KSVD algorithm cannot match all the measurement data. Moreover, simple greedy algorithms (MP, OMP) used in the sparse coding stage have high computational complexity. With network training, the DK-SVD algorithm in this paper can provide the corresponding optimal model parameters for each set of measurement data, thereby improving the imaging quality. Moreover, the ISTA algorithm is used in the sparse coding stage, which greatly improves the convergence speed.

3. MODEL CONSTRUCTION FOR DK-SVD

3.1. Patch Decomposition

The global image sparsification is changed to patch image sparsification, which enables local image features to be captured effectively for DK-SVD method. Due to the irregularity of the imaging area of the EIT image, a patch decomposition method suitable for different image shapes is proposed in this paper. This method utilizes overlapping patches so that the equalization effect is generated, and the image artifacts are reduced.

The local properties of the 2D reconstruction need to be preserved during the sparse representation. Therefore, the EIT image vector needs to be rearranged according to the position of each pixel to form a two-dimensional image. The image is processed in patches, with the size of $\sqrt{p} \times \sqrt{p}$. In this paper, a zero-padding method is proposed to solve the square patch decomposition problem, where the overlap step R denotes the distance between corresponding pixels in adjacent image patches. Let $R = 1$. The method has the following 5 steps (Figure 1):

1) The maximum lengths (expressed by the number of pixels) of the X-axis and Y-axis of the object field are determined. For example, the maximum length of the X-axis is denoted as $N_{x\,\max}$, and the maximum length of the Y-axis is denoted as $N_{y\,\max}$.

2) Let a rectangular area of size $N_{x\,\max} \times N_{y\,\max}$ be constructed. The reconstructed image is contained inside the square area.

3) In the rectangular area, the pixels belonging to the measured object field are marked with 1, and the other parts are marked with 0.

4) Let the entire rectangular area be traversed by square patches of size $\sqrt{p} \times \sqrt{p}$ with overlapping stride R.

5) For all patches, if each pixel in the patch is marked as 1, the patch is classified as a valid patch; if there are pixels marked as 0 in the patch, it is classified as an invalid patch.
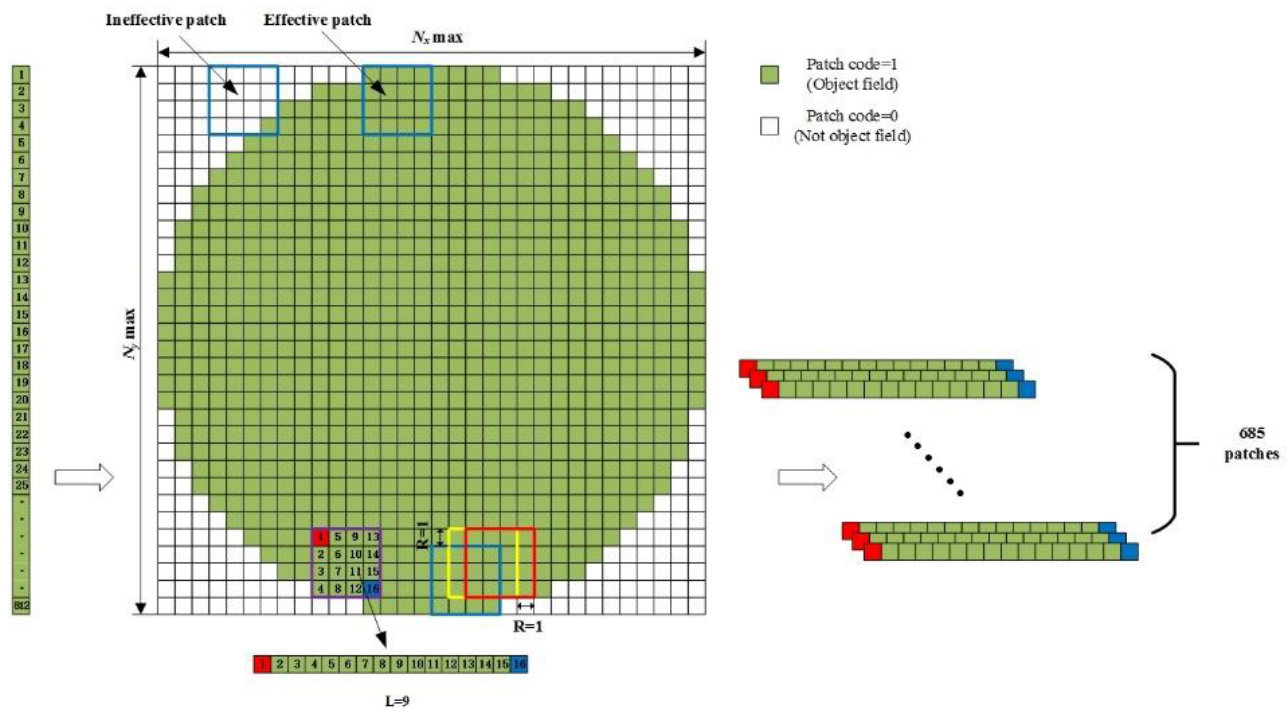

Figure 1. Patching principle for EIT image. It shows an example of a 32×32 square grid.

3.2. Mathematical Model of the New Method

The DK-SVD imaging algorithm proposed in this paper is mainly divided into two parts. The first part is patch sparse coding and parameter learning; the second part is image reconstruction. The sparse imaging process of electrical impedance based on DK-SVD is shown in Figure 2. First, the voltage is initialized as a conductivity image by using the CG algorithm. Then the image is divided into patches, which are sparsely reconstructed to reduce noise. Finally, all the patches are reconstructed through weighted average, so that the whole image can be obtained. The bottom part in the green line box is the details of patch denoising. The optimal regularization parameter is matched to each patch through the network learning method, then the ISTA algorithm is used to solve the sparse coding model so that the sparse coefficients and dictionary are obtained.
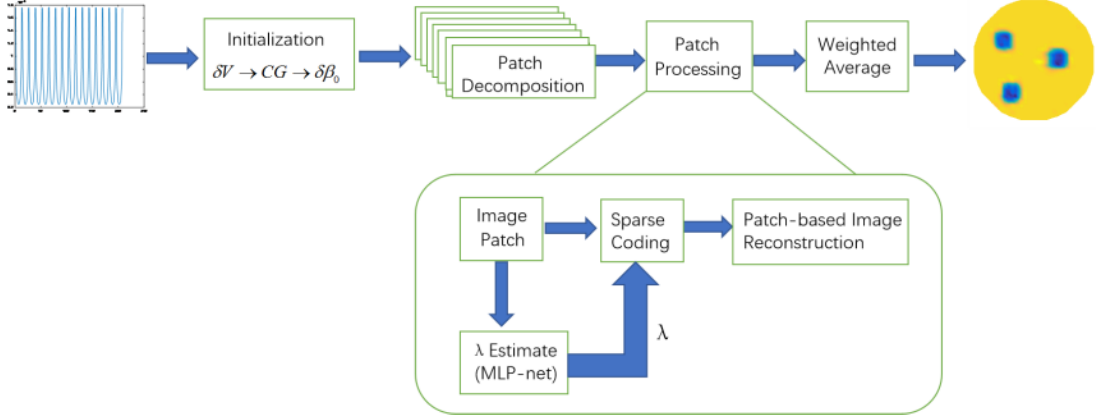
Figure 2. Flow chart of electrical impedance sparse imaging based on DK-SVD.

A possible formula to find the optimum compatible with the measured voltages is:

$$\min_{\{\phi_i\}_i, \delta\beta, Z} \frac{\mu}{2} \left\| \delta\beta - \delta\beta^0 \right\|_2^2 + \sum_i \left(\lambda_i \left\| \phi_i \right\|_1 + \frac{1}{2} \left\| Z\phi_i - R_i\delta\beta \right\|_2^2 \right) \tag{1}$$

where $\delta\beta$ (unknown, of size $(\sqrt{N} \times \sqrt{N})$ represents a noise-free global EIT image. Suppose that the initial $\delta\beta$ is equal to $\delta\beta^0$ (Obtained by Conjugate Gradient (CG) algorithm [34]). $R_i\delta\beta$ ($\sqrt{p} \times \sqrt{p}$) denotes the i-th EIT image patch in $\delta\beta$. Sparse coding and parameter learning are represented in the second term of (1). This entry guarantees that every position of $\delta\beta$ is traversed by $R_i\delta\beta$.

3.3. Algorithm

The solution of formula (1) mainly includes two steps: 1) The input EIT image patches are fixed, and patch sparse coding and parameter learning are performed. 2) The sparse coefficients and dictionary are fixed, and the optimal reconstruction result is obtained through multiple iterations.

3.3.1. Patch Sparse Coding and Parameter Learning

Since the l_1 regularization method tends to produce a sparse solution, it is always used for sparse reconstruction of EIT [35, 36].

The sparse solution model of the i-th patch corresponding to the sparse term in (1) is shown in (2):

$$\hat{\phi}_i = \arg\min_{\phi_i} \frac{1}{2} \left\| Z\phi_i - \delta\beta_i \right\|_2^2 + \lambda_i \left\| \phi_i \right\|_1 \tag{2}$$

where $\mathbf{Z} \in R^{L \times S}$ represents a sparse dictionary. $\hat{\phi}_i$ denotes the sparse coefficient corresponding to the i-th image patch $\delta\beta_i$. λ_i denotes a regularization parameter.

The input EIT image patches are fixed, then the dictionary and sparse representation of the patches are jointly learned. A popular and effective algorithm for solving the above problem is the ISTA [37], which is guaranteed to converge to the global optimum.

$$\hat{\phi}_{t+1} = soft_{\lambda_i/e}\left(\hat{\phi}_t - \frac{1}{e}Z^T\left(Z\hat{\phi}_t - \delta\beta_i\right)\right) \tag{3}$$

where $\hat{\phi}_0 = 0$, e is the squared spectral norm of Z. $soft_{\lambda_i/e}$ is the soft threshold operation function.

$$[soft_\theta(\mathbf{x})]_j = \text{sign}(x_j)(|x_j| - \theta)_+ \tag{4}$$

The distribution of each image patch has different characteristics, so the optimal regularization coefficients corresponding to the image patches are also different. The accuracy of EIT image feature extraction is reduced if the same fixed parameters are used for all image patches. Therefore, adaptive parameters are used in this paper. Consider having a learnable version of the ISTA algorithm generated. Let e, Z, and λ_i be learned during the solution process. That is to say, each λ_i is matched to the corresponding image patch.

Referring to the model in (1), an important issue is the need to set the parameter λ_i. We should set λ_i for each patch so as to yield sparse representation with a controlled level of error. In this paper, a regression function is established from the image patch $\delta\beta_i$ to its corresponding regularization parameter λ_i.

In this paper, the relationship between image patch $\delta\beta_i$ and regularization parameter λ_i is mapped by an MLP network [38, 39], where Θ is the vector of MLP parameters.

$$\lambda_i = f_\Theta(\delta\beta_i) \tag{5}$$

The input layer, hidden layer, and output layer are included in the MLP network. The network structure using the MLP network to solve the regularization parameter λ_i is shown in Figure 3.
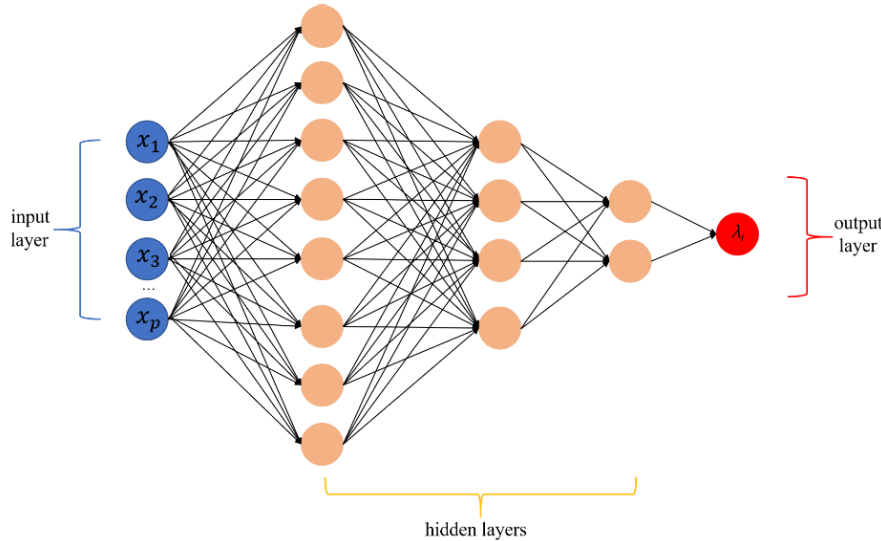
Figure 3. Schematic diagram of MLP network structure. The blue column is the input layer, the three orange columns are hidden layers, the red column is the output layer.

The input layer has p nodes, which is the dimension of the vectorized patch. The regularization parameter λ_i corresponding to the image patch $\delta\beta_i$ is obtained at the output layer. Three hidden layers are included in the MLP network. Each hidden layer consists of a fully connected linear map and ReLU (rectified linear unit) function (except the last layer). ReLU is used as an activation function:

$$H(x) = \begin{cases} 0 \ (x < 0) \\ x \ (x \geq 0) \end{cases} \tag{6}$$

The application of ReLU can alleviate the phenomenon of overfitting and vanishing gradient. The network introduces sparsity through ReLU for better feature extraction and fitting to training data. Suppose that $[f \times d]$ represents a matrix of size $f \times d$. The process of making the regularization parameter λ_i learned by the MLP network can be expressed as: $\delta\beta_i \to [p \times 2p] \to ReLU \to [2p \times p] \to ReLU \to [p/2 \times 1] \to \lambda_i$.

3.3.2. Image Reconstruction

The dictionary Z obtained from (3) and the sparse coefficient $\hat{\phi}_i$ of the EIT image patches are fixed and updated $\delta\hat{\beta}_i$. The problem to be solved is shown in (7):

$$\delta\hat{\beta}_i = \arg\min_{\delta\beta_i} \frac{\mu}{2} \left\| \delta\beta_i - \delta\beta_i^0 \right\|_2^2 + \frac{1}{2} \left\| Z\hat{\phi}_i - R_i\delta\beta \right\|_2^2 \tag{7}$$

(7) is a simple quadratic problem that can be simplified to:

$$\delta\hat{\beta}_i = \left(R_i^T R_i + \mu I \right)^{-1} \left(\mu\delta\beta_i^0 + R_i^T Z\hat{\phi}_i \right) \tag{8}$$

Since the diagonal matrix is included in the matrix required to be inverted, the calculation in (8) is considered to be very simple.

To effectively minimize the cost function in (1), $\hat{\phi}_i$ and $\delta\hat{\beta}_i$ are updated multiple times until the optimal result is produced.

It is worth mentioning that after all $\delta\hat{\beta}_i$ are updated, the reconstruction result is obtained by a linear combination of weighted $\delta\hat{\beta}_i$

$$\delta\hat{\beta} = \frac{\sum_i R_i^T \left(\omega \odot R_i\delta\hat{\beta} \right)}{\sum_i R_i^T \omega} \tag{9}$$

where $\omega \in R^{\sqrt{p} \times \sqrt{p}}$ denotes the weight of $\delta\hat{\beta}_i$.

3.4. Dataset

The dataset consists of boundary voltage measurements and corresponding true conductivity vectors. However, it is difficult to obtain that in an experimental system. Therefore, COMSOL Multiphysics is used in this paper to obtain the simulation model. The conductivity distribution of the model is set according to the conductivity of the lungs. The conductivity of the background (a mixture of fat and tissue fluid) is 0.424 S/m. The conductivity of navy blue and light blue inclusions are set to 0.705 S/m and 0.525 S/m, respectively. The working method of adjacent excitation adjacent measurement is adopted. When all electrodes have been excited, the voltage measurements with 208 elements can be obtained by the finite element method. The true conductivity distribution with a resolution of 32×32 is also obtained from the model.

Six types of samples shown in Figure 4 are made. Different numbers of circles and squares of different sizes were included in the samples. The radius of the circle in the defect is 0.5 cm and 0.9 cm, respectively, and the side length of the square is 1 cm. A total of 24,000 samples were made by randomly simulating inclusions of different numbers, positions, and shapes. A sampling method is used so that the samples are divided into disjoint training and test sets. That is, the training samples are not included in the test samples. Among them, 20,000 samples are included in the training set, and 4,000 samples are included in the test set.

4. RESULTS AND ANALYSIS

4.1. Evaluation Index

Relative error (RE) is an indicator that reflects the deviation of the reconstructed image from the ground truth. Structural similarity index measurement (SSIM) refers to the similarity of brightness, contrast,

---

Algorithm 1 Pseudo code to reconstruct EIT images from measured voltage using DK-SVD.

Input: δV — EIT measured voltage

Output: $\delta\hat{\beta}$ — Reconstructed conductivity distribution

Initialization: $\delta\beta^0$ — Using the CG algorithm to obtain the initial conductivity

$\quad\quad\quad\quad\quad$ Z — Overcomplete discrete cosine transform (DCT) dictionary

$\quad\quad\quad\quad\quad$ $\sqrt{p} \times \sqrt{p}$ — Size of each image patch

$\quad\quad\quad\quad\quad$ $\hat{\phi}_0$ — Initial sparsity coefficient, $\hat{\phi}_0 = 0$

Step1: Update dictionary Z and sparse coefficients $\hat{\phi}_i$ through alternate iterations for image patch reconstruction

1) Sparse coding and regularization parameter learning
   Using the ISTA algorithm and building a perceptron network with three hidden layers
   $\quad$ for each ISTA algorithm iteration:
   $\quad\quad$ for each patch:
   $\quad\quad\quad$ using MLP-Net to get the regularization parameter with the best fit
   $\quad\quad$ for the sparse solution model in (2):
   $\quad\quad\quad$ using (3) to solve (2), updating the dictionary Z and sparse coefficients $\hat{\phi}_i$

2) Patch-based image reconstruction
   The dictionary Z and sparse coefficients $\hat{\phi}_i$ for the EIT image patch are fixed, $\delta\hat{\beta}_i$ is reconstructed based on (7)
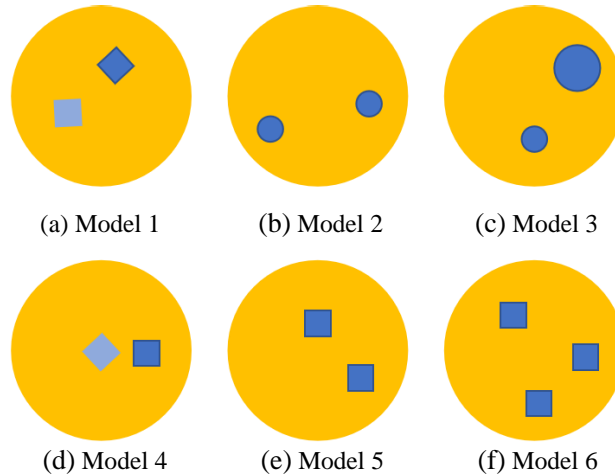   (8) is used to solve problem

Step2: Rebuild the global image

1) for all the updated Z and $\hat{\phi}_i$
   $\quad$ using (1) to reconstruct the global image

2) Take the weighted average of all patches. Obtain final solution $\delta\hat{\beta}$ based on (9).

(a) Model 1   (b) Model 2   (c) Model 3

(d) Model 4   (e) Model 5   (f) Model 6

Figure 4. Sample types.

and structure between two images. In this study, RE and SSIM are adopted to evaluate the quality of reconstruction, as shown in (10) and (11):

$$\text{RE} = \frac{\left\| \delta\hat{\beta} - \delta\beta^* \right\|_2}{\left\| \delta\beta^* \right\|_2} \tag{10}$$

$$\text{SSIM}\left(\delta\beta^*, \delta\hat{\beta}\right) = \frac{\left(2\mu_{\delta\beta^*}\mu_{\delta\hat{\beta}} + D_1\right)\left(2\sigma_{\delta\beta^*\delta\hat{\beta}} + D_2\right)}{\left(\mu_{\delta\beta^*}^2 + \mu_{\delta\hat{\beta}}^2 + D_1\right)\left(\sigma_{\delta\beta^*}^2 + \sigma_{\delta\hat{\beta}}^2 + D_2\right)} \tag{11}$$

where $\delta\beta^*$ denotes the true conductivity image. $\mu_{\delta\beta^*}$ and $\mu_{\hat{\alpha}}$ denote the average of $\delta\beta^*$ and $\delta\hat{\beta}$, respectively. $\sigma_{\delta\beta^*}$ and $\sigma_{\delta\hat{\beta}}$ denote the standard deviation of $\delta\beta^*$ and $\delta\hat{\beta}$, respectively. $\sigma_{\delta\beta^*\delta\hat{\beta}}$ is the covariance of $\delta\beta^*$ and $\delta\hat{\beta}$. D_1 and D_2 represent constants and are used to avoid division by zero.

4.2. Performance Evaluation of Different Patch Sizes

In the DK-SVD method, different patch sizes make the reconstructed images exhibit different qualities. In the patch sparse process, a reasonable patch size should be selected so that the optimal result can be obtained. The reconstructed image errors of the DK-SVD method using different patch sizes are shown in Figure 5. The relative errors of Model 1, Model 2, and Model 3 all decrease as the patch size increases from 3×3 to 9×9. As the patch size increases, the relative error of Model 4 and Model 5 firstly decreases and then increases. Taken together, a patch size of 6×6 enables the relative minimum of RE to be generated. In this paper, 6×6 patches are selected for image reconstruction.

4.3. Running Time Comparison

Table 1 compares the reconstruction times of K-SVD and DK-SVD algorithms. Since the optimal parameters of formula (1) can be obtained through deep learning, the number of iterations for the DK-SVD algorithm is dramatically reduced compared with the K-SVD algorithm. According to the experiment results of typical models, the iteration times of the K-SVD and DK-SVD algorithms are selected as 100 and 50, respectively. In terms of imaging speed, a computer with Intel(R) Core(TM) i5-10400F processor and 16G memory is used for reconstruction. It can be seen that the DK-SVD algorithm takes less time than the K-SVD algorithm.

Table 1. Computational time of two imaging algorithms.

Simulation model	Running time(s)	
	KSVD algorithm	DK-SVD algorithm
Model 1	31.97	22.36
Model 2	30.61	23.34
Model 3	30.33	23.64
Model 4	32.04	22.52
Model 5	30.88	22.94
Model 6	31.88	23.59

4.4. Comparison of Reconstruction Results

Figure 6 shows the reconstruction results of the four methods. The reconstruction results show that the DK-SVD algorithm can better preserve the details and reduce the degree of artifacts than the other three algorithms.

White Gaussian noise with $50\,\text{dB}$ is added to the test set for testing the anti-noise ability of the algorithm. We select random six groups of reconstruction results shown in Figure 7. The DK-SVD algorithm shows good anti-noise ability for gaussian noise with $50\,\text{dB}$, which is enough to deal with common noise and outliers in measurements of the EIT system. However, it is not sensitive enough for the detection of multi-object inclusions which have different conductivities.
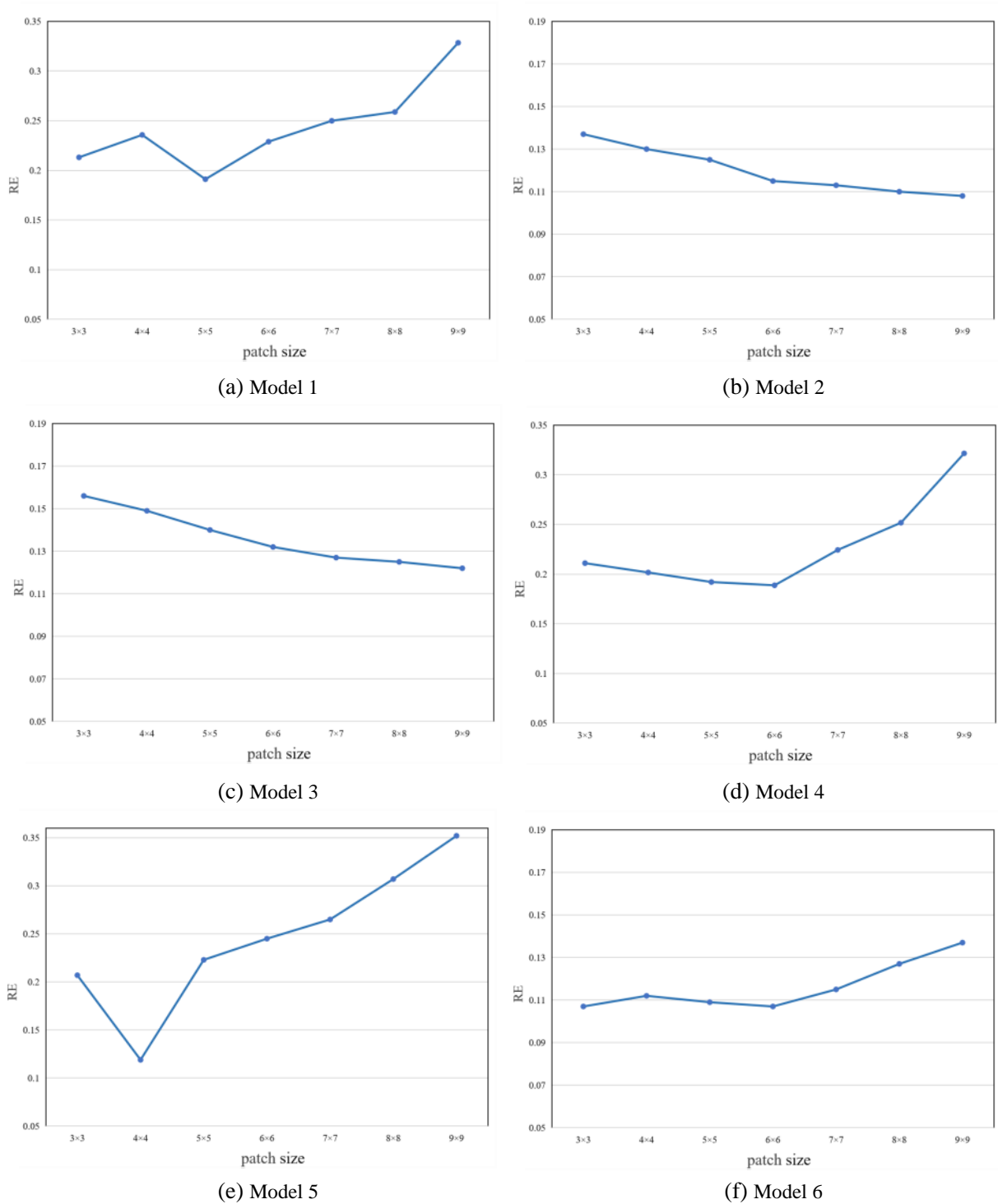
(a) Model 1

(b) Model 2

(c) Model 3

(d) Model 4

(e) Model 5

(f) Model 6

Figure 5. RE values of different patches for 6 models.

4.5. Relative Error and Structural Similarity Assessment

The RE and SSIM of reconstruction images are calculated separately and are given in Figure 8. DK-SVD has the best reconstruction performance.
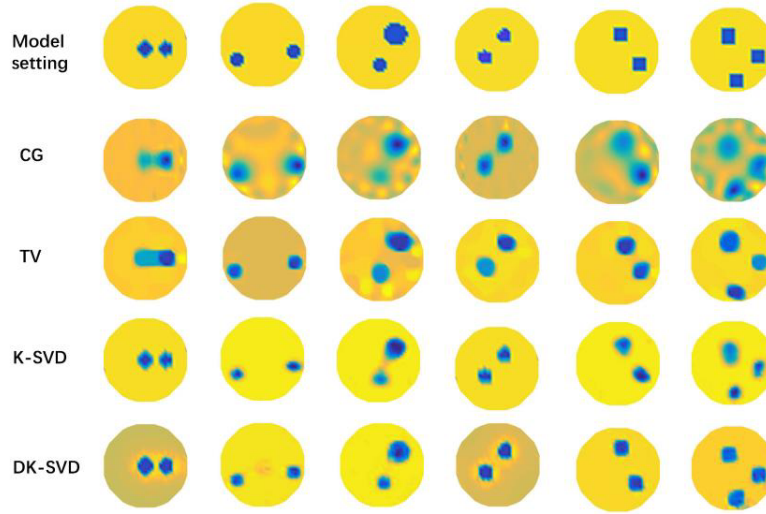
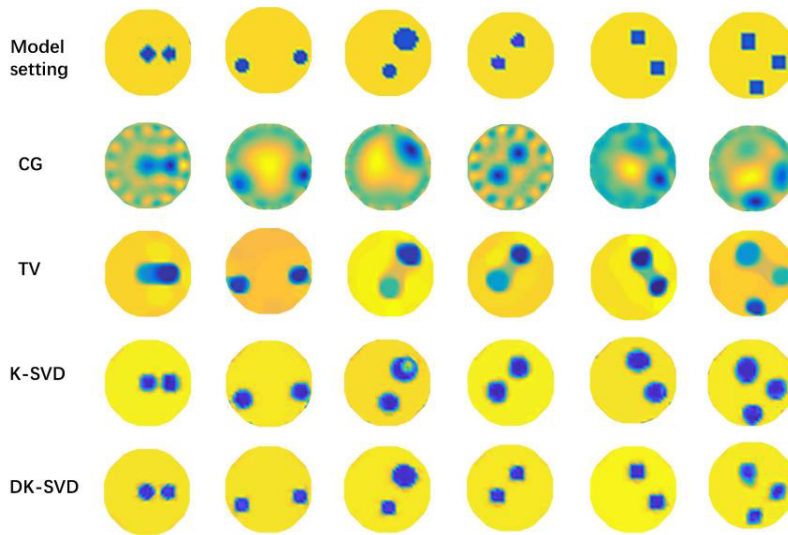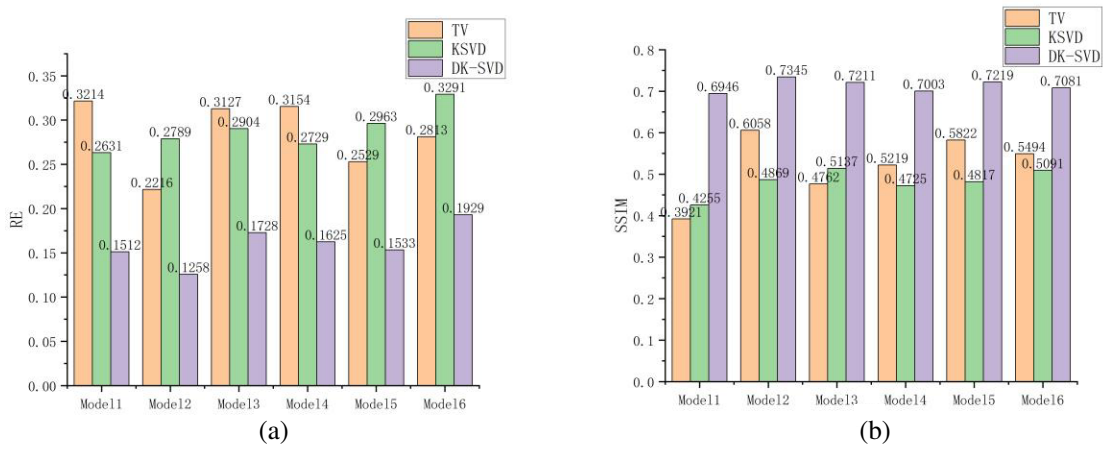**Figure 6.** The reconstruction results of the four methods.

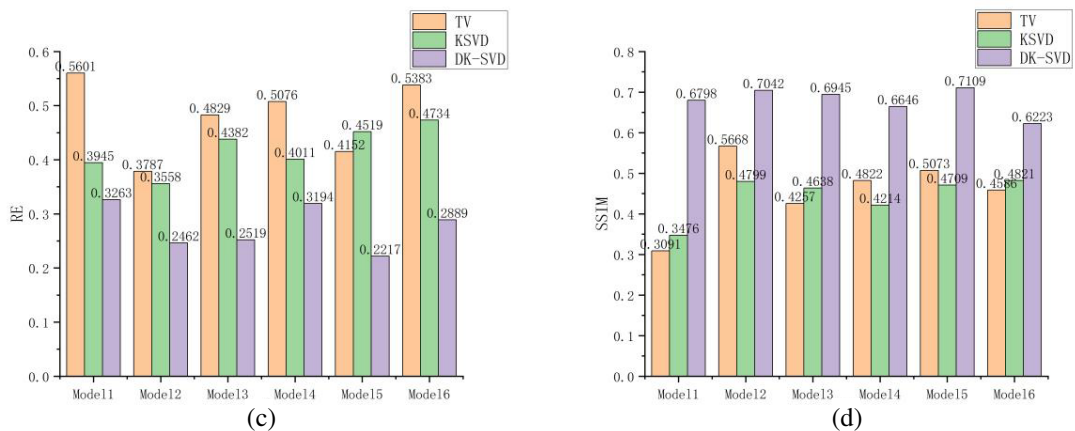**Figure 7.** The reconstruction results of the four methods under 50 dB noise.

(a)   (b)

Figure 8. RE and SSIM of reconstruction images. (a), (b) represent the noise-free case. (c), (d) represent the 50 dB noise case.

5. CONCLUSION

In this paper, a sparse imaging method of electrical impedance tomography based on DK-SVD is proposed. Simulation results have shown that the proposed method not only improves the quality of the image but also enhances the imaging speed by the number of iterations being decreased. For inclusions of different shapes and conductivities, the new algorithm can perform effective reconstruction and has good generalization ability. It means that the proposed method has the potential of improving the speed and accuracy of EIT imaging. In the future, we will simulate the conductivity distribution according to specific scenarios (such as medical and industrial use, etc.) and conduct experimental verification of the new method.

REFERENCES

1. Hong, S., K. Lee, U. Ha, H. Kim, Y. Lee, Y. Kim, and H.-J. Yoo, "A 4.9 mΩ-sensitivity mobile electrical impedance tomography IC for early breast-cancer detection system," *IEEE Journal of Solid-State Circuits*, Vol. 50, No. 1, 245–257, 2015.

2. Fabrizi, L., A. McEwan, T. Oh, E. J. Woo, and D. S. Holder, "A comparison of two EIT systems suitable for imaging impedance changes in epilepsy," *Physiological Measurement*, Vol. 30, No. 6, S103–S120, 2009.

3. Nissinen, A., J. P. Kaipio, M. Vauhkonen, and V. Kolehmainen, "Contrast enhancement in EIT imaging of the brain," *Physiological Measurement*, Vol. 37, No. 1, 1–24, 2016.

4. Jang, G. Y., G. Ayoub, Y. E. Kim , T. I. Oh, C. R. Chung, G. Y. Suh, and E. J. Woo, "Integrated EIT system for functional lung ventilation imaging," *BioMedical Engineering OnLine*, Vol. 18, No. 1, 1–18, 2019.

5. Bradley, D. and J. Bagnell, "Differential sparse coding," *Proc. Conf. Neural Information Processing Systems*, 2008.

6. Wang, J., J. Yang, K. Yu, F. Lv, T. Huang, and Y. Gong, "Locality-constrained linear coding for image classification," *2010 IEEE Computer Society Conference on Computer Vision and Pattern Recognition*, 3360–3367, 2010.

7. Zylberberg, J., J. T. Murphy, and M. R. DeWeese, "A sparse codingmodel with synaptically local plasticity and spiking neurons can account for the diverse shapes of V1 simple cell receptivefields," *PLOS Comput. Biol.*, Vol. 7, No. 10, e1002250, 2011.

8. Davis, G., S. Mallat, and M. Avellaneda, "Adaptive greedy approximations," *J. Construct. Approx.*, Vol. 13, 57–98, 1997.

9. Aharon, M., M. Elad, and A. Bruckstein, "K-SVD: An algorithm for designing overcomplete dictionaries for sparse representation," *IEEE Transactions on Signal Processing*, Vol. 54, No. 11, 4311–4322, Nov. 2006, doi: 10.1109/TSP.2006.881199.

10. Yang, J., Y. Zhang, and W. Yin, "A fast alternating direction method for TVL1-L2 signal reconstruction from partial fourier data," *IEEE Journal of Selected Topics in Signal Processing*, Vol. 4, No. 2, 288–297, 2010.

11. Needell, D. and R. Vershynin, "Signal recovery from incomplete and inaccurate measurements via regularized orthogonal matching pursuit," *IEEE Journal of Selected Topics in Signal Processing*, Vol. 4, No. 2, 310–316, 2010.

12. Wang, Q., Z. Lian, J. Wang, Q. Chen, Y. Sun, X. Li, X. Duan, Z. Cui, and H. Wang, "Accelerated reconstruction of electrical impedance tomography images via patch based sparse representation," *Review of Scientific Instruments*, Vol. 87, No. 11, 114707, 2016.

13. Wang, Q., P. Zhang, J. Wang, Q. Chen, Z. Lian, X. Li, Y. Sun, X. Duan, Z. Cui, B. Sun, and H. Wang, "Patch based sparse reconstruction for electrical impedance tomography," *Sensor Review*, Vol. 37, No. 3, 257–269, 2017.

14. Li, X., J. Zhang, J. Wang, Q. Wang, and X. Duan, "Recursive least squares dictionary learning algorithm for electrical impedance tomography," *Progress In Electromagnetics Research C*, Vol. 97, 151–162, 2019.

15. Wang, C., D. Sun, and K. C. Toh, "Solving log-determinant optimization problems by a Newton-CG primal proximal point algorithm," *Siam Journal on Optimization*, Vol. 20, No. 6, 2994–3013, 2009.

16. Hou, W. and Y. Mo, "Image reconstruction in electrical impedance tomography based on genetic algorithm," *Shengwu Yixue Gongchengxue Zazhi/Journal of Biomedical Engineering*, Vol. 20, No. 1, 107–110, 2003.

17. Marquina, A. and S. Osher, "Image super-resolution by TV-regularization and Bregman iteration," *Journal of Scientific Computing*, Vol. 37, No. 3, 367–382, 2008.

18. Yu, C., S. Fan, Y. Bo, and D. Chen, "A novel quasi-newton image reconstruction algorithm for electrical capacitance tomography system," *2009 ISECS International Colloquium on Computing, Communication, Control, and Management*, 89–93, 2009.

19. Dai, T. and A. Adler, "Electrical impedance tomography reconstruction using l_1 norms for data and image terms," *2008 30th Annual International Conference of the IEEE Engineering in Medicine and Biology Society*, 2721–2724, 2008.

20. Gehre, M., T. Kluth, A. Lipponen, B. Jin, A. Seppänen, J. P. Kaipio, and P. Maassa, "Sparsity reconstruction in electrical impedance tomography: An experimental evaluation," *Journal of Computational and Applied Mathematics*, Vol. 236, No. 8, 2126–2136, 2012.

21. Gehre, M., T. Kluth, C. Sebu, and P. Maass, "Sparse 3D reconstructions in electrical impedance tomography using real data," *Inverse Problems in Science & Engineering*, Vol. 22, No. 1, 31–44, 2014.

22. Theertham, G. T., S. K. Varanasi, and P. Jampana, "Sparsity constrained reconstruction for electrical impedance tomography," *IFAC-PapersOnLine*, Vol. 53, No. 2, 355–360, 2020.

23. Liu, S., R. Cao, Y. Huang, T. Ouypornkochagorn, and J. Jia, "Time sequence learning for electrical impedance tomography using bayesian spatiotemporal priors," *IEEE Transactions on Instrumentation and Measurement*, Vol. 69, No. 9, 6045–6057, 2020.

24. Shi, Y., Y. Wu, M. Wang, Z. Tian, X. Kong, and X. He, "Sparse image reconstruction of intracerebral hemorrhage with electrical impedance tomography," *Journal of Medical Imaging*, Vol. 8, No. 1, 014501, 2021.

25. Hu, G., J. Lin, G. Wang, and R. He, "Sparse reconstruction based channel estimation for underwater piezo-acoustic backscatter systems," *2021 IEEE 93rd Vehicular Technology Conference (VTC2021-Spring)*, 1–5, 2021.

26. Li, S., H. Wang, J. N. Chen, and Z. Cui, "An improved sparse reconstruction algorithm based on singular value decomposition for electrical resistance tomography," *2021 IEEE International Instrumentation and Measurement Technology Conference (I2MTC)*, 1–6, 2021.

27. Kou, S. and X. Feng, "Angle-micro-Doppler frequency image of underwater target multi-highlight combining with sparse reconstruction," *Applied Acoustics*, Vol. 188, 108563, 2022.

28. Donoho, D. L., "Compressed sensing," *IEEE Trans. Inf. Theory*, Vol. 52, 1289–1306, Apr. 2006.

29. Ye, J. M., H. G. Wang, and W. Q. Yang, "Image reconstruction for electrical capacitance tomography based on sparse representation," *IEEE Transactions on Instrumentation and Measurement*, Vol. 64, No. 1, 89–102, Jan. 2015.

30. Jin, B., T. Khan, and P. Maass, " A reconstruction algorithm for electrical impedance tomography based on sparsity regularization," *Int. J. Numer. Methods Eng.*, Vol. 89, 337–353, Jan. 2012.

31. Qu, X. B., Y. Hou, F. Lam, D. Guo, J. H. Zhong, and Z. Chen, "Magnetic resonance image reconstruction from undersampled measurements using a patch-based nonlocal operator," *Med. Image Anal.*, Vol. 18, 843–856, Aug. 2014.

32. Elad, M. and M. Aharon, "Image denoising via sparse and redundant representations over learned dictionaries," *IEEE Trans. Image Process.*, Vol. 12, 3736–3745, 2006.

33. Wang, Q., K. Sun, J. Wang, and R. Zhang, "Reconstruction of EIT images via patch based sparse representation over learned dictionaries," *2015 IEEE International Instrumentation and Measurement Technology Conference (I2MTC) Proceedings*, 2044–2048, 2015.

34. Wang, M. and W. Yin, "Electrical impedance tomography," US06940286B2, 2005.

35. Donoho, D. L. and M. Elad, "Optimally sparse representation in general (nonorthogonal) dictionaries via l_1 minimization," *Proc. Nat. Acad. Sci. USA*, Vol. 100, No. 5, 2197–2202, Mar. 2003.

36. Donoho, D. L., M. Elad, and V. N. Temlyakov, "Stable recovery of sparse overcomplete representations in the presence of noise," *IEEE Trans. Inf. Theory*, Vol. 52, No. 1, 6–18, Jan. 2006.

37. Daubechies, I., M. Defrise, and C. D. Mol, "An iterative thresholding algorithm for linear inverse problems with a sparsity constraint," *Commun. Pure Appl. Math.*, Vol. 57, No. 11, 1413–1457, 2004.

38. Xiang, C., S. Ding, and T. H. Lee, "Geometrical interpretation and architecture selection of MLP," *IEEE Transactions on Neural Networks*, Vol. 16, No. 1, 84–96, 2005, doi:10.1109/tnn.2004.836197.

39. Lacrama, D. L., V. Gherhes, F. Alexa, and T. M. Karnyanszky, "Automatic survey processing using a MLP neural net," *10th Symposium on Neural Network Applications in Electrical Engineering*, 123–126, 2010.